Pramana – J. Phys. (2022) 96:68
https://doi.org/10.1007/s12043-022-02316-z

Intermediate length scale of water jets under gravity: An experimental result

WELLSTANDFREE K BANI[1,2] and MANGAL C MAHATO[1,*]

[1]Department of Physics, North-Eastern Hill University, Shillong 793 022, India
[2]Department of Physics, Synod College, Shillong 793 002, India
*Corresponding author. E-mail: mangal@nehu.ac.in

MS received 28 July 2021; revised 5 October 2021; accepted 22 November 2021

Abstract. The profile of water jets along its length before breakup is indirectly inferred from the observation of surface waves created by the jet as it plunges into a reservoir of pure and contaminated water. The inference is drawn based on the measurement of surface wavelengths as a function of jet length before it touches the reservoir surface. It is observed that the nature of variation of wavelength changes abruptly at a certain jet length L_0. It is found that the dimensionless L_0 depends only on the local velocity and diameter of the jet at $L = L_0$ apart from the local acceleration due to gravity but is not a function of the surface tension of the reservoir; i.e., L_0 is a function of the Froude number Fr at $L = L_0$. Our analysis suggests the existence of an intermediate length scale L_0 that demarcates the inertia-dominated region ($L < L_0$) of the jet from the gravity-dominated region ($L > L_0$).

Keywords. Water jet; under gravity; capillary waves; gravity/surface waves; fluid pipe.

PACS Nos 47.60.-i; 47.20.Dr; 47.35.Pq

1. Introduction

A jet is formed as water flows down a vertically oriented nozzle of a small horizontal cross-section of radius r_0 under gravity at a flow rate Q greater than the critical rate Q_c [1]. The vertical jet flowing down under its own weight breaks up into drops at a mean distance $L = L_B$ from the nozzle exit. The breakup length $L = L_B$ of the jet is usually a monotonically increasing function of flow rate Q. The length L_B for viscous liquids like silicon oil can be as large as 10 m whereas L_B for water is usually less than 10 cm [2]. The understanding of this ubiquitous phenomenon is still a continuing saga, though notable advances have been made beginning with the famous Plateau–Rayleigh theory [3,4]. These advances have been described well in some recent reviews [5,6] and many other important publications [2,7–15] to cite but a few among the representative ones.

Most of the works on jets describe conditions of breakup of axisymmetric unconfined jets. Hancock and Bush [13] and Martinez-Calvo *et al* [14] investigated jets confined between the point of their emergence at the mouth of the nozzle and the surface of the liquid in the reservoir placed on the path of the jet when length $L < L_B$. Martinez-Calvo *et al* [14] explained the condition of stability of confined viscous liquid jets in their steady and oscillatory regimes, occurring at different values of L as a function of Q, discovered earlier in unconfined jets [11]. In ref. [13], clean water jets were allowed to impinge on the liquid surface in a reservoir containing, separately, clean water and dilute water-detergent solution. The authors observed the resulting capillary waves on the clean water jets in the case of clean water reservoir and also in solution reservoir. However, in the case of solution reservoir, 'fluid pipes' appeared above the liquid surface in the reservoir and the capillary waves showed up above the entry point of the fluid pipe. In the present work, we describe and explain our experimental results on confined clean water jets as in the case of ref. [13].

There has been a spurt of activity recently in this field of research on account of the potential technological applications of viscous jets and significant results have been obtained on the gravitationally stretched jets [2,7,8,12]. For example, Javadi *et al* [2] confirmed the important role played by viscosity in determining the large breakup length L_B of a gravitationally stretched jet, resolving an earlier paradox that L_B

Published online: 29 March 2022

should be independent of viscosity η [8]. This work has been elaborated and extended in ref. [12] including the perturbations introduced at the nozzle mouth as well as the noise present throughout the jet length for a larger range of viscosity paramaters. The analysis predicts the functional dependence of the jet breakup length L_B.

The major focus of these works have justifiably been on explaining and/or measuring the breakup length of the jets. However, before the jet reaches its point of breakup, its profile may undergo changes in many ways along the jet-length. In certain regions of the jet-length, the profile may be determined by the jet-fluid surface tension, its viscosity and/or local acceleration due to gravity, local jet speed u and radius r. The inertia effect may thus also come into reckoning. In the present experimental work, an intermediate length scale L_0 was identified demarcating a region of jet length ($L < L_0$) dominated by inertia effect from the region ($L > L_0$) dominated by the gravity effect. This sharp point L_0 of demarcation occurs well before the jet-breakup point $L = L_B$.

The earlier works of high-speed photography of the water jets show that necks and bulges form as one moves down along the length of the jet with increasing separation between two consecutive bulges [16]. We do not have the means to undertake similar exercise to ascertain the profile of the jet around $L = L_0$. However, without providing any experimental evidence, we presume that the jet profile must have necks and bulges before it reaches $L = L_0$ because L_0 turns out to be larger than $L_B/2$.

As has been mentioned earlier, when an axisymmetric continuous clean water jet falling under gravity impinges on the surface of the same liquid in the reservoir, capillary waves can be observed on the jet closer to the surface of the liquid in the reservoir. However, when the jet impinges on the surface of a reservoir of liquid of lower surface tension, jet 'fluid pipes' appear close to the liquid surface in the reservoir and the capillary waves show up only above the fluid pipe [13]. It is not clear, however, whether these capillary waves have any relationship with the Rayleigh capillary perturbation waves. As in the above described work, in the present work too, jets of clean water were allowed to impinge on the reservoir of clean water and also on the reservoirs of dilute water solutions of various concentrations of commercially available Tide detergent. However, in addition to observing and measuring the wavelengths λ_c of the capillary waves, the concomitant waves produced on the liquid surface in the reservoir were observed and their wavelengths λ_s were measured. It is the nature of variation of λ_s as a function of the jet-length L that provides the clue to the existence of the intermediate length scale L_0 as discussed in the following sections.

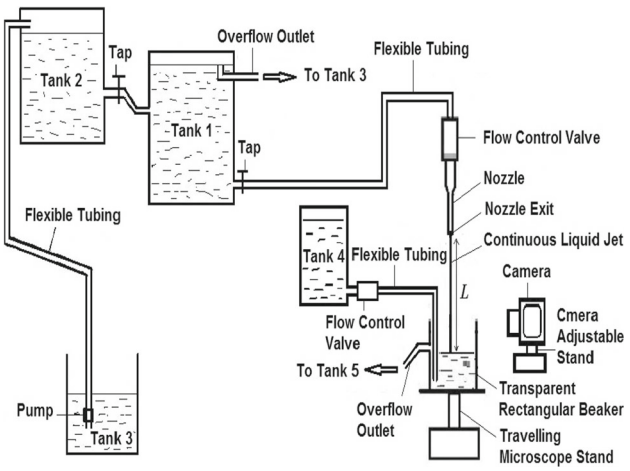

Figure 1. The diagrammatic sketch of the experimental set-up.

2. Experimental set-up and experiment

The basic experimental set-up used in the present work to obtain clean water jet through a nozzle essentially remains the same as explained elsewhere [17,18]. However, a small modification has been made in the measuring method and reservoir part of the set-up to serve our present purpose, as shown in figure 1. The vertical jet impinges smoothly on a constant level reservoir containing either clean water (as in the jet) or a water solution of Tide detergent. For the purpose of having a reservoir containing water solution of various concentrations c of Tide detergent, we added an extra tank (Tank 4) containing water solution of concentration $2c$. As the clean water jet impinges on the reservoir at a flow rate Q, we continuously added solution to the reservoir from the extra tank at the same rate Q so that the concentration of the solution in the reservoir remains fixed at c. However, the surface level in the reservoir remains constant as the extra solution always flows out through a side level-tube fixed to the vertical side of the reservoir. Utmost care was taken not to disturb the liquid surface while adding the solution from the extra tank.

The reservoir (beaker containing the solution) was placed on a horizontal platform fitted to the vertical stand of a travelling microscope (vernier scale least count=0.001 cm). The experiment involves stationing the reservoir vertically below the nozzle at various heights so that the vertical distance L of the horizontal surface of the reservoir from the mouth of the nozzle

can be smoothly changed as required. In other words, the length L of the continuous jet was measured and fixed at a desired value. As the continuous jet meets the liquid surface in the reservoir and merges with it, two phenomena are observed: (1) in the case of clean water reservoir, only capillary waves are generated on the liquid jet and in the case of water-detergent solution reservoir, both fluid pipe and capillary waves are generated and (2) waves are created on the liquid surface in the reservoir. These waves (and fluid pipes) were photographed using an ordinary (Nikon D5300) camera. The digitally stored photographs were then analysed with the help of a personal computer (after proper calibration) to obtain wavelengths λ_c and λ_s of the capillary and surface waves and heights (H) of the fluid pipes at various values of jet length L. Typical photographs are shown in figure 2 (for surface waves) and figures 3 and 4 (for capillary waves and fluid pipe).

The surface tension σ of the clean and contaminated water was carefully measured using the Jaeger's method at various concentrations c and tabulated. The flow rate Q was measured manually. The tap water was distilled once to obtain 'clean' water to be used in the experiment. The same clean water was used to prepare the water-detergent solutions. All the measurements were done at the room temperature of (25 ± 0.5)°C and at a relative humidity of (80 ± 4)%. For our calculations, however, we used the tabulated values of the dynamic viscosity $\eta = 8.9 \times 10^{-3}$ g cm^{-1} s^{-1} and density $\rho = 0.997$ g cm^{-3} of water and the local acceleration due to gravity $g = 980$ cm s^{-2}.

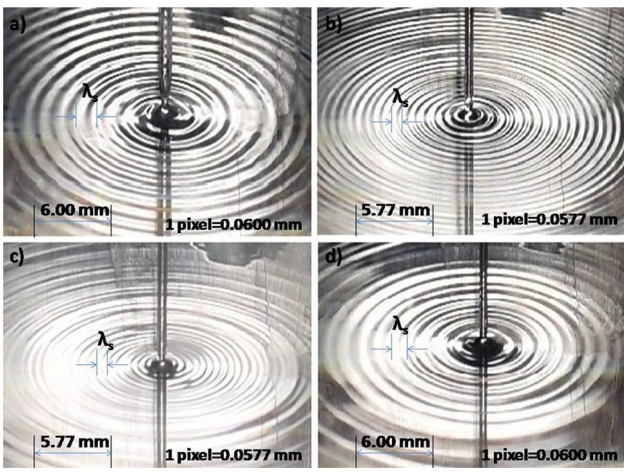

Figure 2. Photograph of waves on clean water ($c = 0$ mg cm^{-3}) reservoir surface at jet lengths (**a**) $L = 0.168$ cm, (**b**) $L = 0.568$ cm, (**c**) $L = 3.618$ cm and (**d**) $L = 4.268$ cm. The experimental parameters are: $r_0 = 0.047$ cm and $Q = 0.833$ cm^3 s^{-1}.

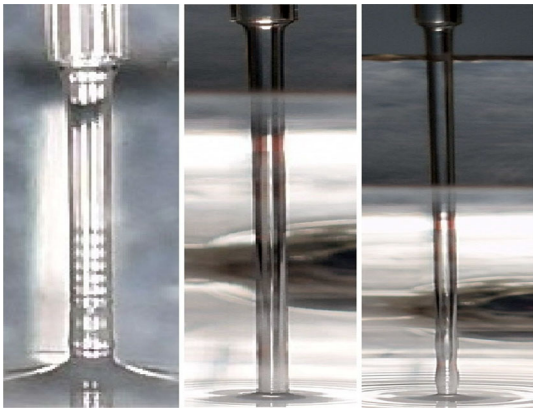

Figure 3. Photograph of capillary waves and fluid pipes when a clean water jet is impinging on the reservoir surface contaminated with Tide detergent solution ($c = 1$ mg cm^{-3}). The experimental data from left to right are respectively for $L = 1.074$ cm, $L = 3.500$ cm and $L = 4.900$ cm. Here, $r_0 = 0.047$ cm and $Q = 0.833$ cm^3 s^{-1}. Note that the jet develops necks and bulges before $L = L_B$ (see the right photo).

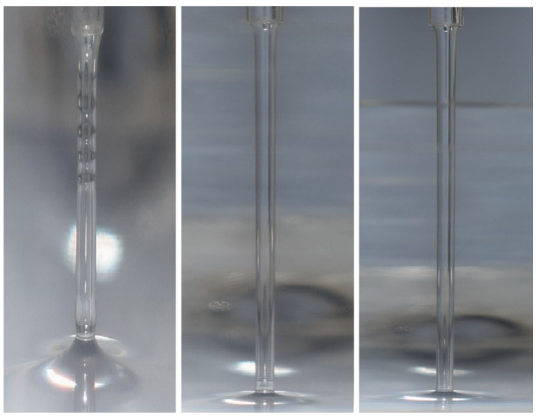

Figure 4. Photograph of capillary waves and fluid pipe when a clean water jet is impinging on the reservoir surface contaminated with Tide detergent solution ($c = 5$ mg cm^{-3}). The experimental data from left to right are respectively for $L = 0.850$ cm, $L = 3.550$ cm and $L = 5.050$ cm. Here, $r_0 = 0.047$ cm and $Q = 0.667$ cm^3 s^{-1}. Note that the jet does not develop necks and bulges before $L = L_B$ (see the right photo).

3. Experimental results

In our experiment, we used nozzles of various internal diameters $d_0 = 2r_0$ at their mouth, for example, $d_0 = 0.095$ cm, 0.126 cm, 0.154 cm, 0.178 cm, etc. and limited flow rates so that we should not face difficulty in measuring the jet length since the vertical stand of the travelling microscope has limited length. For each of these nozzles, we performed our experiment at various flow rates Q. Therefore, the mean jet velocity u_0 at

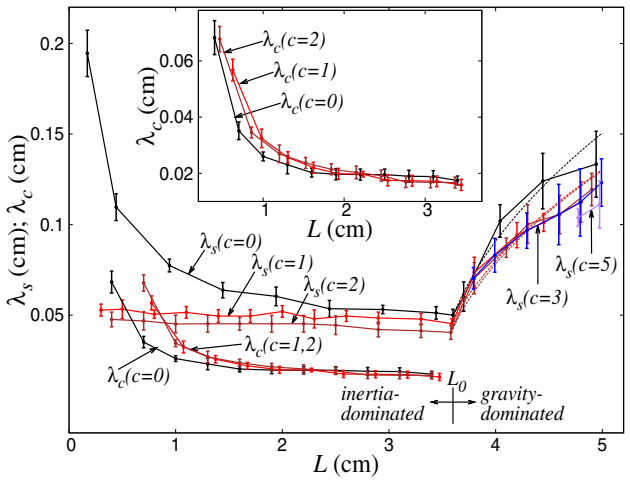

Figure 5. Plots of wavelengths $\lambda_s(c = 0)$, $\lambda_s(c = 1)$, $\lambda_s(c = 2)$, $\lambda_s(c = 3)$ and $\lambda_s(c = 5)$ of surface waves on the reservoir of clean water $c = 0$, and at detergent concentrations of $c = 1$, $c = 2$, $c = 3$ and $c = 5$ mg cm^{-3}, and wavelengths $\lambda_c(c = 0)$, $\lambda_c(c = 1)$ and $\lambda_c(c = 2)$ of capillary waves as a function of jet-length L. λ_s are numerically fitted (dashed lines), respectively, with $0.05\sqrt{1 + \frac{980}{170}(L - 3.6)}$, $0.04534\sqrt{1 + \frac{980}{190}(L - 3.59)}$ and $0.04048\sqrt{1 + \frac{980}{150}(L - 3.58)}$. The experimental parameters are: $r_0 = 0.047$ cm and $Q = 0.833$ cm^3 s^{-1}. The inset shows that the three λ_cs overlap when the fluid pipe length correction is taken (see text). Note that the wavelengths $\lambda_s(c = 3)$ and $\lambda_s(c = 5)$ of surface waves on the reservoir seem to appear at $L > L_0$.

the mouth of the nozzle can be calculated as

$$u_0 = \frac{4Q}{\pi d_0^2} = \frac{Q}{\pi r_0^2}.$$

All the sets of experiment show similar results from which one can draw similar conclusions. Therefore, for brevity, we present our typical results when a nozzle of $d_0 = 0.095$ cm was used at a convenient flow rate $Q = 0.833$ cm^3 s^{-1}. The results are summarised in figure 5 where the measured wavelengths λ_s and λ_c are plotted as a function of jet length L when the reservoir contained (1) clean water ($c = 0$), water-detergent solution of concentration (2) $c = 1$ mg cm^{-3} and (3) concentration $c = 2$ mg cm^{-3}. Figure 5 has several noteworthy features as follows.

For clean water ($c = 0$), the surface wavelength λ_s as a function of L initially decreases monotonically till the jet length $L = L_0$ and then λ_s sharply increases till the jet breaks up at $L = L_B$ into drops. The surface waves in the water-detergent solution reservoir show the same behaviour (with approximately the same value of L_0 within the experimental error bars) except that λ_s remains almost constant till $L = L_0$. Interestingly, for $L > L_0$ one is tempted to think that the surface waves might have been generated due to the necks and bulges of the jet profile whose separation increases with increasing jet length due to gravitational effect [12] whereas for $L < L_0$ the surface waves might have been generated due to impingement of the smooth surface (underdeveloped necks and bulges) with reducing cross-sectional area of the jet due to inertia. The surface waves for $L < L_0$ is essentially similar to the circular surface waves produced when a fishing line of uniform cross-sectional area is pushed into (or pulled from) the surface of water [19]. This is also supported by the formation of necks and bulges of the jet as a function of jet length for different concentrations of Tide detergent solution in the reservoir as shown in figures 3 and 4. In the spirit of ref. [20], and considering λ_s to be proportional to the difference in the jet length between two consecutive bulgings, we numerically fit $\lambda_s(L)$ as

$$\lambda_s(L) = \lambda_s(L_0)\sqrt{1 + \frac{2g(L - L_0)}{v_0^2}},$$

taking v_0 as a fitting parameter for $c = 0$, 1 and 2 mg cm^{-3}. As can be seen from figure 5, the fit is reasonable. We could similarly fit the data for all the other nozzles in a range of flow rates.

As in ref. [13], we observe fluid pipes when $c \neq 0$ just above the liquid surface in the reservoir. Of course, in all the cases, the jet comes in contact with the liquid surface in the reservoir with a bulbous smear. Also, as explained in ref. [13], the water-detergent solution of lower surface tension (than clean water) ascends the surface of the jet forming the fluid pipe. Above the fluid pipe, it is just the clean water jet where capillary waves are formed. Therefore, the capillary wave λ_c should have the same nature with a jet length correction due to the fluid pipe length H: $\lambda_c(L, c = 0) \approx \lambda_c(L - H, c \neq 0)$. These values of λ_c with the mentioned length correction are replotted in the inset of figure 5, showing that the three curves almost overlap with each other.

The capillary waves seem to persist beyond $L = L_0$. However, their amplitude is too feeble that it cannot be measured with the camera at our disposal. When $L < L_0$, it appears that there is some weak correlation between the behaviour of λ_s and λ_c, at least for $c = 0$. However, there is definitely no such correlation when $L > L_0$. Therefore, it is reasonable to assume that the two waves have different physical origins. We conjecture that capillary waves may be due to the average impulsive elastic reaction of the liquid surface in the reservoir on the impinging jet, whereas surface waves are a signature of the spatiotemporal jet profile. The fluid pipe effectively strips the jet of its profile details

Table 1. Measured values of surface tension σ for different concentrations c of Tide detergent in water solution.

c (mg cm^{-3})	0.0	1.0	2.0	3.0	4.0	5.0
σ (g s^{-2})	70.11 ± 0.46	48.43 ± 0.14	43.06 ± 0.14	38.95 ± 0.22	36.66 ± 0.18	34.76 ± 0.22

Table 2. Experimentally measured values of flow rate Q (cm^3 s^{-1}), internal radius r_0 (cm) of the nozzle and the length L_0 (cm) of the jet and the calculated values of the ratio L_0/r and the corresponding dimensionless Weber number We $= \rho u^2 r/\sigma$, Bond number Bo $= \rho r^2 g/\sigma$, Ohnesorge number Oh $= \nu\sqrt{\rho/r\sigma}$ and Froude number Fr $= u/\sqrt{2gr}$ using the values of local jet speed $u = \sqrt{u_0^2 + 2gL_0}$ and local jet radius $r = r_0\sqrt{u_0/u}$ at $L = L_0$.

Measured values			Calculated values				
Q	r_0	L_0	L_0/r	We	Bo	Oh	Fr
0.667	0.047	3.618	88.245	9.292	0.023	0.006	14.083
0.750		3.558	84.544	10.874	0.025	0.006	14.842
0.833		3.600	84.021	12.721	0.026	0.006	15.767
0.950		3.542	80.916	15.503	0.027	0.006	17.038
0.958	0.063	4.763	95.821	10.774	0.034	0.005	12.508
1.083		4.760	92.391	12.366	0.037	0.005	12.928
1.208		4.795	90.521	14.154	0.039	0.005	13.453
1.333		4.770	87.913	16.036	0.041	0.005	13.980
1.458		4.720	85.249	18.054	0.043	0.005	14.536
1.167	0.077	5.773	105.253	11.885	0.042	0.005	11.906
1.500		5.720	95.476	15.076	0.050	0.005	12.276
1.667		5.870	95.249	17.100	0.053	0.005	12.710
1.833		5.710	89.850	18.869	0.056	0.005	12.947
2.000		5.806	89.524	21.128	0.059	0.005	13.425
2.167		5.760	87.057	23.353	0.061	0.005	13.835
1.917	0.089	6.700	100.793	18.021	0.062	0.005	12.097
2.167		6.800	98.463	20.535	0.066	0.005	12.429
2.417		6.800	95.228	23.111	0.071	0.005	12.752
2.667		6.800	92.632	25.901	0.075	0.004	13.132
2.917		6.750	89.773	28.835	0.079	0.004	13.527
3.167		6.798	88.751	32.152	0.082	0.004	14.022

and hence the surface waves almost do not show variation of λ_s for $c = 1$ and 2 mg cm^{-3} with L and the surface waves disappear for $c = 3$ and 5 mg cm^{-3} below $L = L_0$. Above $L = L_0$, however, the fluid pipes essentially disappear for $c = 1$ and 2 mg cm^{-3} and hence λ_s shows characteristic sharp increase with L, as in the case of $c = 0$ mg cm^{-3} but persist even though it is feeble for $c = 3$ and 5 mg cm^{-3} and hence λ_s appears at $L > L_0$. This could be because the necks and bulges of the unstable jet dominate over the fluid pipe at $L = L_0$ for $c = 1$ and 2 mg cm^{-3} and far larger than $L = L_0$ (becoming closer to $L = L_B$) as the concentration c of the Tide detergent solution is increased.

Within the experimental error, the values of L_0 are the same for all the values of c plotted in figure 5. In table 1, the measured values of surface tension σ at various detergent concentrations of the water-detergent solution are given. It is clear that the surface tensions are very different at different values of c. It, therefore, follows that L_0 does not depend on surface tension σ. Though we have not measured the viscosity η of the solutions, we believe that they will also be different at different values c and hence L_0 should be independent of η as well. With these experimental information at hand, we analyse our experimental results concerning L_0 for various parameter values of nozzle internal diameters d_0 and flow rates Q as follows.

We calculate the local radius r and velocity u of the jet at various lengths L of the jet in general and at $L = L_0$ in particular, using their respective values r_0 and u_0 at the mouth of the nozzle as

$$u = \sqrt{u_0^2 + 2gL},$$

and

$$r = r_0\sqrt{\frac{u_0}{u}},$$

as used in ref. [21]. When $L = L_0$, these local values may be considered as some kind of average valuesover

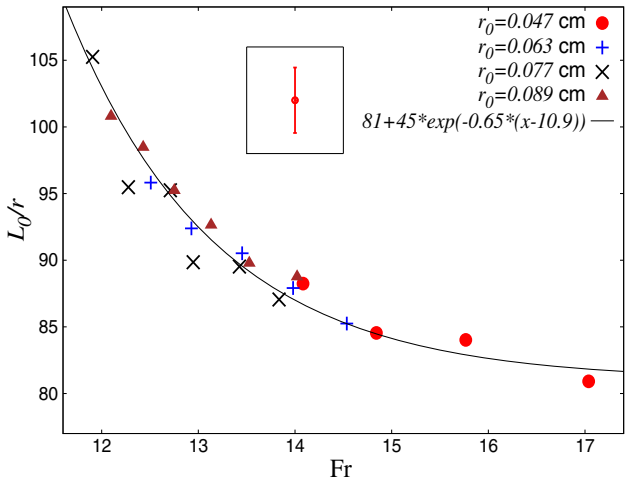

Figure 6. Plot of the dimensionless length L_0/r as a function of the Froude number Fr. Each point on the graph corresponds to a combination of parameters r_0 and Q given in table 2. A typical length of the error bars is separately shown in the graph. The line is arbitrarily drawn to guide the eye.

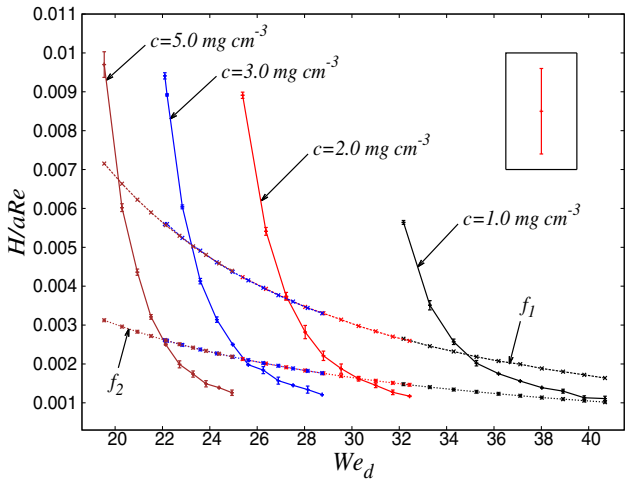

Figure 7. Plot of dimensionless fluid pipe height (H/aRe) and its approximate expressions $f_1 = 2.73/\mathrm{We}_d{}^2$ (dashed upper curve) and $f_2 = \frac{2.73}{\mathrm{We}_d{}^2}\left(1 + \frac{25.1}{\mathrm{We}_d} + \frac{0.879}{S\mathrm{We}_d{}^2}\right)^{-1}$ (dotted lower curve) as a function of the dynamic Weber number ($\mathrm{We}_d = \rho a V^2/\Delta\sigma$), where the Stokes number $S = \nu V/ga^2$, Reynolds number $\mathrm{Re} = aV/\nu$, H is the the height of the fluid pipe and V is the entry speed at the entrance of the fluid pipe ($V = u(L-H)$; $a = r(L-H)$). The experimental parameters are: $r_0 = 0.047$ cm, $Q = 0.833$ cm^3 s^{-1}, $c = 1$, $c = 2$, $c = 3$, $c = 5$ mg cm^{-3} and $S \approx 0.58$–0.79. The inset shows the maximum diameter of the bulbous base of the fluid pipe that connects to the surface of the reservoir. Note that the height of the fluid pipe H is measured till $L = L_0$.

a distance of two consecutive bulgings of the jet. Buckingham's Π-theorem, therefore, allows us to perform dimensional analysis taking u, r (or $d = 2r$), ρ and g as independent physical quantities and L_0 as a dependent physical quantity [22,23]. The dimensional analysis readily yields

$$\frac{L_0}{d} = f\left(\frac{u^2}{gd}\right), \tag{1}$$

where $f(x)$ is some function of x. Therefore, the dimensionless length L_0 is a function only of the local jet diameter d, local jet speed u and the local acceleration due to gravity g. Note that the Froude number Fr is given by

$$\mathrm{Fr} = \frac{u}{\sqrt{gd}}.$$

Thus, the dimensionless L_0 is a function of Fr only.

In table 2, we tabulate the experimentally measured values of flow rate Q (cm^3 s^{-1}), the internal radius at the mouth of the nozzle r_0 (cm), L_0 (cm), the calculated values of local jet speed u (cm s^{-1}), local radius r (cm), L_0/r, the dimensionless numbers We, Bo, Oh and Fr calculated at $L = L_0$ when the reservoir has clean water. Figure 6 shows plot of L_0/r as a function of the Froude number Fr for all the nozzle radii r_0 and flow rates Q. It can be seen that all the data points approximately fall on a single curve exhibiting the correctness of our result of the dimensional analysis, eq. (1). The plots of L_0/r as a function of either the Weber number $\mathrm{We} = \rho u^2 r/\sigma$ or the Bond number $\mathrm{Bo} = \rho r^2 g/\sigma$ do not show such dimensional similarity. The Ohnesorge number $\mathrm{Oh} = \nu\sqrt{\rho/r\sigma}$, where the kinematic viscosity $\nu = \eta/\rho$, is orders of magnitude smaller than other dimensionless numbers and expect not to show any dimensional similarity.

It can also be noticed from table 2 that the measured L_0 are not the same for a given r_0 corresponding to various flow rates Q, but are nearly the same. When values of L_0 are averaged over the flow rates for given r_0, one obtains roughly a straight line, that is, the ratio of mean $\overline{L_0}$ and r_0 turns out to be a constant (≈ 76). However, this does not give any information about the nature of jet profile at L_0.

The plots of dimensionless fluid pipe height (H/aRe, where the Reynolds number $\mathrm{Re} = aV/\nu$ and H is the height of the fluid pipe) as a function of the dynamic Weber number ($\mathrm{We}_d = \rho a V^2/\Delta\sigma$, V is the entry speed at the entrance of the fluid pipe $V = u(L-H)$; $a = r(L-H)$) for different concentrations c and flow rates Q are shown in figures 7 and 8. It can be seen that for smaller jet length, the experimental values of the height of the fluid pipe is closer to $f_1 = 2.73/\mathrm{We}_d{}^2$ where the effect of gravity on the height of the fluid pipe is ignored but as the jet length is increased ($L \approx L_0$) the height of

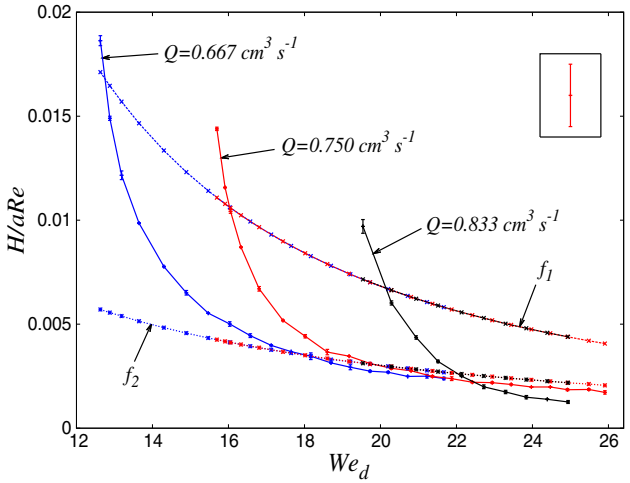

Figure 8. Plot of the dimensionless fluid pipe height ($H/a\mathrm{Re}$) and its approximate expressions $f_1 = 2.73/\mathrm{We}_d{}^2$ (dashed upper curve) and $f_2 = \frac{2.73}{\mathrm{We}_d{}^2}\left(1 + \frac{25.1}{\mathrm{We}_d} + \frac{0.879}{S\mathrm{We}_d{}^2}\right)^{-1}$ (dotted lower curve) as a function of the dynamic Weber number ($\mathrm{We}_d = \rho a V^2/\Delta\sigma$). The experimental parameters are: $r_0 = 0.047$ cm, $c = 5$ mg cm^{-3}, $Q = 0.667$, $Q = 0.750$, $Q = 0.833$ cm^3 s^{-1} and $S \approx 0.46$–0.99. The inset shows the maximum diameter of the bulbous base of the fluid pipe that connects the fluid pipe to the surface of the reservoir. Note that the height of the fluid pipe H is measured beyond $L = L_0$.

the fluid pipe becomes closer to

$$f_2 = \frac{2.73}{\mathrm{We}_d{}^2}\left(1 + \frac{25.1}{\mathrm{We}_d} + \frac{0.879}{S\mathrm{We}_d{}^2}\right)^{-1}$$

and the Stokes number $S = \nu V/ga^2$ where the effect of gravity on the height of the fluid pipe is taken under consideration [13]. Our measured lengths of the fluid pipe are not in agreement with the earlier more precise results of Hancock and Bush. In our experiment, we have used the Stokes number $S \approx 0.46$–0.99 which is large and more scattered than the mean Stokes number $S \approx 0.062$ used in [13]. However, these changes of $H/a\mathrm{Re}$ from f_1 to f_2 as a function of We_d with increasing jet length (as the jet length L approaches L_0) may be due to the increase of local jet speed and thus the speed at the entrance of the fluid pipe. Admittedly, our experimental results are not as accurate as those of Hancock and Bush and we analysed the results using $\nu = 0.009$ cm^2 s^{-1} to calculate the Stokes number S.

4. Conclusion

We performed an experiment to observe the effect of clean water jet impinging into clean water (and also water-detergent dilute solution) reservoir surfaces situated at intermediate distances between the mouth of jet-emanating nozzles and the jet's breakup distance under gravity. The resulting capillary waves on the jets (and also fluid pipes in the case of solution reservoirs) and the waves produced on the reservoir surfaces are observed using an ordinary camera. Naturally, given the experimental facility available at our disposal, the error bars are not very small. However, the error bars are too small to obscure our qualitative conclusions: (i) that there is no correlation between the wavelengths of the capillary wave and the surface wave, at least for $L > L_0$ and (ii) that there exists a definite intermediate length scale L_0 of the jet where the nature of its profile changes from inertia-dominated region to the gravity-dominated region as described by the dimensionless Froude number.

References

[1] C Clanet and J C Lasheras, *J. Fluid Mech.* **383**, 307 (1999)
[2] A Javadi, J Eggers, D Bonn, M Habibi and N M Ribe, *Phys. Rev. Lett.* **110**, 144501 (2013)
[3] J Plateau, *Experimental and theoretical statics of liquids subject to molecular forces only* (Gauthier-Villars, Paris, 1873) Vol. 2
[4] Lord J W S Rayleigh, *Proc. Lond. Math. Soc.* **10**, 4 (1879)
[5] J Eggers, *Rev. Mod. Phys.* **69**, 865 (1997)
[6] J Eggers and E Villermaux, *Rep. Prog. Phys.* **71**, 036601 (2008)
[7] U S Sauter and H W Buggisch, *J. Fluid Mech.* **533**, 237 (2005)
[8] S Senchenko and T Bohr, *Phys. Rev. E* **71**, 056301 (2005)
[9] A Umemura, *Phys. Rev. E* **83**, 046307 (2011)
[10] A Umemura, S Kawanabe, S Suzuki and J Osaka, *Phys. Rev. E* **84**, 036309 (2011)
[11] M Rubio-Rubio, A Sevilla and J M Gordillo, *J. Fluid Mech.* **729**, 471 (2013)
[12] S Le Dizes and E Villermaux, *J. Fluid Mech.* **810**, 281 (2017)
[13] M J Hancock and J W M Bush, *J. Fluid Mech.* **466**, 285 (2002)
[14] A Martinez-Calvo, M Rubio-Rubio and A Sevilla, *J. Fluid Mech.* **834**, 335 (2018)
[15] R Mead-Hunter, A J C King and B J Mullins, *Langmuir* **28**, 6731 (2012)
[16] D F Rutland and G J Jameson, *J. Fluid Mech.* **46**, 267 (1971)
[17] W K Bani and M C Mahato, arXiv:1810.09267v1 [physics.flu-dyn] (2018)
[18] W K Bani and M C Mahato, *Pramana – J. Phys.* **95**, 1 (2021)

[19] H Lamb, *Hydrodynamics* (Cambridge University Press, Cambridge, 1895)
[20] L E Scriven and R L Pigford, *AIChE J.* **5**, 397 (1959)
[21] V Grubelnik and M Marhi, *Am. J. Phys.* **73**, 415 (2005)
[22] P W Bridgman, *Dimensional analysis* (Yale University Press, New Haven, 1931)
[23] A A Sonin, *Lecture notes on the physical basis of dimensional analysis* (MIT, Cambridge, 2001)